Mode matching in second-order-susceptibility metal-dielectric structures

Sébastien Héron,[1,2] Patrick Bouchon,[1,*] and Riad Haïdar[1,3]
[1]*MINAO, ONERA, The French Aerospace Lab, 91761 Palaiseau, France*
[2]*MINAO, Laboratoire de Photonique et de Nanostructures, CNRS, Université Paris–Saclay, Route de Nozay, 91460 Marcoussis, France*
[3]*Département de Physique, École Polytechnique, Université Paris–Saclay, 91128 Palaiseau, France*
(Received 26 February 2016; published 19 September 2016)

We present an effective-medium model for a subwavelength periodically patterned metallic layer, its cavities being filled with a nonlinear dielectric material, which accounts for both the linear and second-order behavior. The effective nonlinear susceptibility for the homogenized layer is driven by the nonlinearity of the dielectric material and by the geometrical parameters, thus leading to much higher susceptibility than existing materials. This leads to a huge enhancement of nonlinear processes when used together with resonances. Furthermore, multiple resonances are taking place in the metallic cavities and we investigate the mode-matching situations for frequency conversion processes and show how it enhances further their efficiency.

DOI: 10.1103/PhysRevA.94.033831

I. INTRODUCTION

Metamaterials are artificial materials, obtained with subwavelength patterned elements, that exhibit effective electromagnetic properties that depend not only on the material, but also on the geometry. They have given rise to original and unprecedented behaviors in both linear and nonlinear regimes, such as optical cloaking, phase-matched negative index, or left-handed metamaterials [1–3]. Subwavelength patterned elements can behave as nanoantennas able to funnel the incoming light and concentrate it in a small volume, which is extremely appealing in the context of nonlinear optics [4–8]. Indeed, optical nanoantennas can provide huge enhancement of the electric field and even if the volume at stake is small compared to the whole device, nonlinear effects can be boosted. Most of the nanoantennas reported in the literature are metallic, as they can confine the field more easily than dielectric antenna. So the surface nonlinearities of the metal itself are enhanced [5,9–11], even if dielectric materials can provide much-higher-volume nonlinearities.

To establish a nonlinear metamaterial model from a patterned material, one has to exhibit the influence of its geometrical parameters on the linear and nonlinear optical properties. It can be done, for instance, with the Maxwell-Garnett formalism [12], through field averaging [13] or by retrieving it from rigorous computations or experiments [14]. Once it is described as an effective layer, multiple harmonic resonances can be targeted and exploited to have each one of the wavelengths involved in the frequency conversion process resonant. This multiresonance situation is referred to as a mode-matching situation where several cavity modes are excited during the whole nonlinear process. Recently, several metallic mode-matching nanostructures have been suggested to further improve the efficiency of nonlinear effects based on either plasmonic nanoantennas [15,16] or phase-array sources [17].

In this paper we report on mode matching in a high-susceptibility metasurface for frequency conversion. The investigated structure consists of a patterned metallic layer, filled with a nonlinear dielectric, that melts the high-confinement properties of metallic nanoantennas and the high nonlinear susceptibility of chosen dielectric materials. One of the main differences from previously studied plasmonic structures lies in the monitoring of the nonlinear response by the material filling the holes in the metallic layer rather than the metallic surface generation itself. It additionally exhibits multiple Fabry-Pérot resonances that can be used for mode matching. These harmonic resonances are studied in Sec. II. Then Sec. III presents an effective-medium model that fairly accounts for both linear and nonlinear behaviors of the structure. The effective linear and nonlinear optical properties are found to be mainly determined by the aperture ratio. Section IV deals with the ways to achieve mode matching in the case of second-harmonic generation (SHG) and difference frequency generation (DFG), allowing us to reach resonantly enhanced conversion efficiency. These results are scalable to large spectral ranges and can be adapted in the context of metasurfaces based on metal-insulator-metal antennas.

II. LINEAR RESPONSE

We aim at describing both linear and nonlinear behaviors of a subwavelength periodic metal-dielectric layer where the dielectric inclusions display a second-order nonlinear susceptibility. Two configurations of this system are considered, as shown in Fig. 1. In the first case, the metal-dielectric layer is placed upon a metallic substrate, forming a grating of grooves [Fig. 1(a)], and acts as a reflection device. In the other case, the metal-dielectric layer is standing in air, forming a grating of slits [Fig. 1(b)]. The permittivity of the metal ϵ_{m} is considered identical in the layer and the substrate, while the dielectric inclusions bear a permittivity ϵ_{d} and a nonlinear susceptibility tensor $\chi_{\mathrm{d}}^{(2)}$ that contains only $\chi_{iii}^{(2)}$ terms. The incoming wave is normally incident and transverse magnetic (TM) polarized, at the wavelength λ with a wave vector $k_0 = 2\pi/\lambda$. The period d is a subwavelength and the grooves or slits have a height h and a width w.

The nonlinear material, gallium arsenide, is described by a Sellmeier formula, meaning it is lossless in the spectral region of interest 2–10 μm, sufficiently far from the absorption

*patrick.bouchon@onera.fr

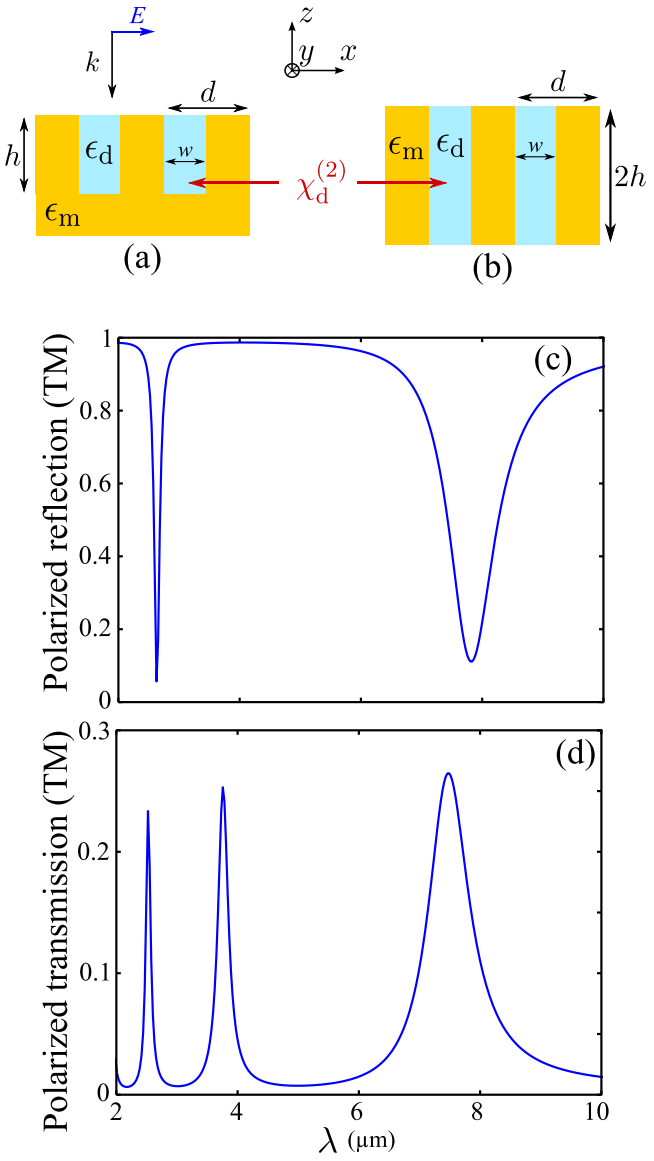

FIG. 1. (a) Periodic grating (period d) of metallic grooves of width w and height h, filled with a nonlinear dielectric acting in reflection (permittivity ϵ_d and nonlinear susceptibility $\chi_d^{(2)}$). (b) Periodic grating of metallic slits filled with a nonlinear dielectric, with parameters similar to those for the reflecting case and acting in transmission. The waves are normally incident and TM polarized with wave vectors **k** lying in the xOz plane. (c) Reflectivity for the reflection resonator and (d) transmissivity for the transmission one, as functions of the wavelength. The parameters are $d = 1$ μm, $w = 200$ nm, and $h = 500$ nm for the reflection case and $h = 1$ μm for the transmission case.

wavelengths:

$$\epsilon_d(\omega) = a_0 + \sum_{l=1}^{3} \frac{a_l}{\omega_l - \omega}, \tag{1}$$

where ω_1, ω_2, and ω_3 correspond to $\lambda_1 = 0.443$ μm, $\lambda_2 = 0.875$ μm, and $\lambda_3 = 36.9$ μm, respectively, and $a_0 = 5.373$, $a_1 = 27.84$, $a_2 = 0.031$, and $a_3 = 0.001$ [18]. The metal, which is gold, is described by a Drude model with a plasma frequency at $\lambda_p = 159$ nm:

$$\epsilon_m(\omega) = 1 - \frac{\omega_p^2}{\omega^2 + i\Gamma\omega}, \tag{2}$$

where $\Gamma = \gamma\omega_p = 0.0048\omega_p$ [19]. The losses are induced by the two metallic surfaces and become higher as the width gets smaller.

Numerical studies show that the optical response of the resonator is a consequence of the guiding of the light inside the slits forming a subwavelength cavity. To determine its resonant wavelengths, the normalized propagation constant of the fundamental mode $\sqrt{\epsilon_{TM}}$ of the plane waveguide set by the two metallic surfaces is deduced from the equation [20]

$$\tanh\left(k_0\sqrt{\epsilon_{TM} - \epsilon_d}\frac{w}{2}\right) = -\frac{\epsilon_d}{\epsilon_m}\sqrt{\frac{\epsilon_{TM} - \epsilon_m}{\epsilon_{TM} - \epsilon_d}}. \tag{3}$$

After some tedious calculations, this equation can be solved at the first order since $|\epsilon_d| \ll |\epsilon_m|$, and ϵ_{TM} is written as

$$\epsilon_{TM} = \epsilon_d\left(1 + \frac{2\delta}{w} - \frac{\epsilon_d}{\epsilon_m}\right), \tag{4}$$

where $\delta = i\lambda/2\pi\sqrt{\epsilon_m}$ is the metal skin depth. The incoming light on the structure is either reflected or funneled into the slit [21,22], so the energy in the metal-dielectric layer is contained in the dielectric inclusions.

As a consequence, the linear response of both structures shows Fabry-Pérot resonances leading to reflectivity dips and transmissivity peaks [see Figs. 1(c) and 1(d)], at wavelengths determined by solving the phase condition inside the cavity

$$\lambda_m = \frac{2\sqrt{\epsilon_{TM}}h^*}{m - \phi/2\pi}, \tag{5}$$

where $m\epsilon\mathbb{N}^*$ and ϕ is the phase of the bottom reflection coefficient. It is equal to zero for the transmission situation and to π for the reflection case. To take into account the penetration of the propagating mode in the bottom metal in the asymmetric case, an equivalent height $h^* = h + \delta$ is introduced in the reflection case and $h^* = h$ in the transmission one. At resonance, the electric-field distributions inside the slits correspond to the establishment of stationary waves inside the guiding slits (see Fig. 2). They are given in the incidence plane at wavelengths corresponding to the normalized harmonic resonances. Exaltation is observed in both reflection and transmission, promising interesting results for nonlinear purposes. The position of the amplitude nodes is predicted by the order of the considered harmonics as in a classical Fabry-Pérot interferometer. Such a description of the system is sustained by the subwavelength feature that implies the funneling effect. Plus, the refractive index of the dielectric filling the cavity is high enough to induce an optical path that allows the presence of stationary waves in spite of the thinness of the component compared to the wavelength.

III. EFFECTIVE-MEDIUM MODEL

The classical effective-medium theory [23] cannot be applied here because the electromagnetic fields are nearly zero inside the metallic region. Energy-conservation considerations are rather used in our case as it was previously suggested for

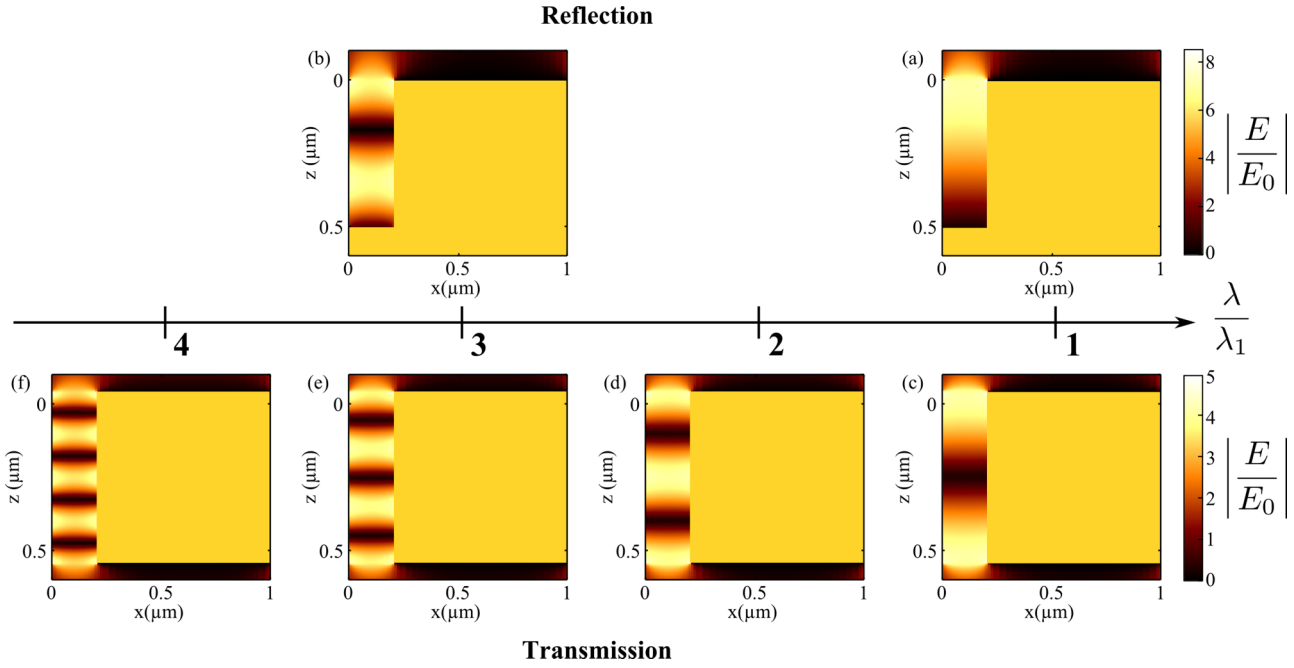

FIG. 2. Electric-field maps inside the slits filled with GaAs for (a) and (b) reflection and (c)–(f) transmission resonators. The maps show the absolute value of the electric field in the incident plane xOz normalized to the incoming one (normally incident TM-polarized plane wave). They are computed at resonant normalized wavelengths λ/λ_1, with λ_1 being the highest resonant wavelength. The parameters are $w = 200$ nm, $d = 1\ \mu$m, and (a) and (b) $h = 500$ nm and (c)–(f) $h = 1\ \mu$m.

the transmission device [see Fig. 3(b)]. It has been described as a metamaterial for perfect metals and involved an effective thickness [24,25]. Here we aim at taking a real lossy metal into account without considering any influence of the thickness h on the constitutive parameters of the effective medium, namely $\bar{\epsilon}$, $\bar{\mu}$, and $\bar{\chi}^{(2)}$. The detailed analytical model treats the grating as a metasurface: It consists of a homogeneous layer of the effective medium of the same height h presenting the same optical properties (see Fig. 3). No effective thickness $\bar{h}$ is used and no prior assumption about this parameter is needed to establish the model. It is shown that varying this value even permits the monitoring of the resonant properties of the structure as these stem from the Fabry-Pérot cavity formed within the slits or grooves.

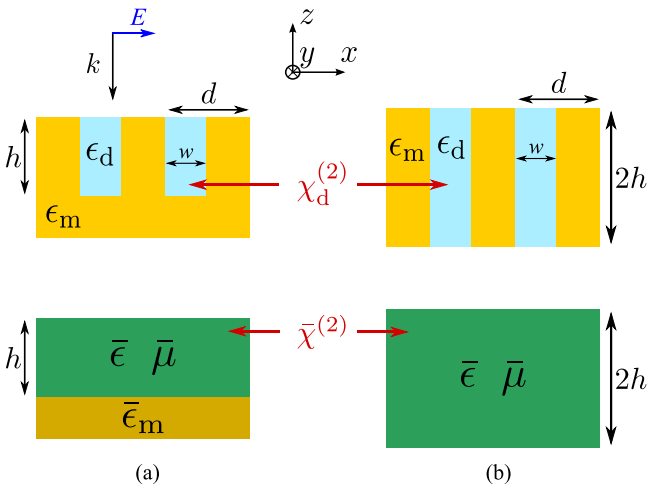

FIG. 3. (a) Reflection case of periodic grating (period d) of metallic grooves of width w and height h, filled with a nonlinear dielectric (permittivity ϵ_d and nonlinear susceptibility $\chi_d^{(2)}$). The waves are normally incident and TM polarized with wave vectors $\mathbf{k}$ lying in the xOz plane. Shown on the bottom is the equivalent effective medium, which consists of a homogeneous layer with effective permittivity, permeability, and nonlinear susceptibility. (b) Transmission case of periodic grating of metallic slits filled with a nonlinear dielectric, with parameters similar to the those in the reflecting case.

A. Dispersive approach

We seek the effective permittivity $\bar{\epsilon}$ and permeability $\bar{\mu}$ of a homogenized layer bearing the same optical response of the structure illuminated by TM-polarized light. The stored energy is the same in the effective layer as in the dielectric part of the resonators. In addition, as the waves are mainly propagating in the dielectric part, the losses of the effective layer are assumed infinitesimal, thus allowing the use of the Landau formula for the internal electromagnetic energy in this dispersive medium [26], here expressed in one subwavelength grating period d,

$$\mathcal{U} = \iint_{x,z} [\partial_\omega(\omega\epsilon(x,z))E(x,z)^2 + \partial_\omega(\omega\mu(x,z))H(x,z)^2]dx\,dz. \quad (6)$$

Stating that the resonator and the effective layer must contain the same amount of energy leads to (with nonmagnetic materials $\mu = 1$)

$$\iint_{x,z} \partial_\omega(\omega\epsilon)E^2 + H^2 = \iint_{x,z} \partial_\omega(\omega\bar{\epsilon})\bar{E}^2 + \partial_\omega(\omega\bar{\mu})\bar{H}^2. \quad (7)$$

In the slits, the TM-polarized light is vertically guided and behaves as a plane wave experiencing an effective permittivity denoted by ϵ_{TM}. This feature is justified by both the funneling effect [21] and numerical field maps that are given at resonance in Fig. 2. We can then make use of the link between the various electromagnetic fields of the plane wave propagating inside the slits, $\epsilon E^2 = \mu H^2$ and $\bar{\epsilon}\bar{E}^2 = \bar{\mu}\bar{H}^2$ (even valid for dispersive media),

$$\iint_{x,z} [\partial_\omega(\omega\epsilon) + \epsilon]E^2 = \iint_{x,z} \left[\partial_\omega(\omega\bar{\epsilon}) + \frac{\partial_\omega(\omega\bar{\mu})\bar{\epsilon}}{\bar{\mu}}\right]\bar{E}^2. \tag{8}$$

The bounds of integration along x are limited to the dielectric since the energy stored in the metallic sidewalls is negligible. Indeed, at the metal-dielectric interface, the x component of the electric field is discontinuous and the normal electric fields on each side are linked by

$$\left|\frac{E_x(x = w^-)}{E_x(x = w^+)}\right| = \left|\frac{\epsilon_{\mathrm{m}}}{\epsilon_{\mathrm{d}}}\right| \gg 1, \tag{9}$$

leading to an amplitude of the electric fields inside the dielectric inclusion that is far greater than that inside the metal. Plus, the fundamental guided mode presents phase and amplitude invariance along the x direction, simplifying the lateral integration. Eventually both the slit resonator and the effective layer have to present Fabry-Pérot resonances (see Fig. 2). Thus, electromagnetic fields have known vertical distributions analogous to stationary-wave amplitudes. Under these circumstances, we obtain at any frequency

$$w[\partial_\omega(\omega\epsilon_{\mathrm{d}}) + \epsilon_{\mathrm{d}}]E^2 = d\left[\partial_\omega(\omega\bar{\epsilon}) + \frac{\partial_\omega(\omega\bar{\mu})\bar{\epsilon}}{\bar{\mu}}\right]\bar{E}^2. \tag{10}$$

In addition, equivalent guiding of the waves means that $\bar{\epsilon}\bar{\mu} = \epsilon_{\mathrm{TM}}$, which can be written as a derivative

$$\partial_\omega(\omega\bar{\mu})\bar{\epsilon} = \frac{\partial_\omega(\omega^2\epsilon_{\mathrm{TM}})}{\omega} - \partial_\omega(\omega\bar{\epsilon})\bar{\mu}, \tag{11}$$

further simplifying Eq. (10),

$$\frac{d}{w}[\partial_\omega(\omega\epsilon_{\mathrm{d}}) + \epsilon_{\mathrm{d}}] = \frac{1}{\bar{\mu}}\frac{\partial_\omega(\omega^2\epsilon_{\mathrm{TM}})}{\omega}, \tag{12}$$

where the confinement property $E/\bar{E} = d/w$ has been used. Indeed, the potential difference inside one period has to be equal between the original configuration and the effective one, so $\bar{E}d = Ew$. The effective permeability is eventually written as

$$\bar{\mu} = \frac{w}{d}\frac{\partial_\omega(\omega^2\epsilon_{\mathrm{TM}})}{\omega[\epsilon_{\mathrm{d}} + \partial_\omega(\omega\epsilon_{\mathrm{d}})]}, \tag{13}$$

with $\bar{\epsilon}$ being obtained from $\bar{\epsilon}\bar{\mu} = \epsilon_{\mathrm{TM}}$. In addition, by assuming negligible dispersion at the first order for the derivatives of the permittivities ϵ_{d} and ϵ_{TM}, we retrieve the following expression:

$$\bar{\mu}_1 = \frac{w}{d}\frac{\epsilon_{\mathrm{TM}}}{\epsilon_{\mathrm{d}}}, \quad \bar{\epsilon}_1 = \frac{d}{w}\epsilon_{\mathrm{d}}. \tag{14}$$

The absence of an imaginary part in $\bar{\epsilon}_1$ means that electric losses are negligible, which is consistent with the fact that the electric energy is strictly confined in the dielectric region described by a Sellmeier model. The losses are essentially magnetic as the induction field penetrates the metallic sidewalls of the slit.

B. Nondispersive approach

Further calculations show that the nondispersive approach for the expression of the internal electromagnetic energy suffices to retrieve expressions of Eq. (14). In this case, the energy conservation between the gratings and the effective layer gives

$$\int_{z=0}^{z=h}\int_{x=0}^{x=d} \bar{\mathbf{E}}\cdot\bar{\mathbf{D}} = \int_{z=0}^{z=h}\int_{x=0}^{x=w} \mathbf{E}\cdot\mathbf{D}, \tag{15}$$

where $\mathbf{D}$ is the electric displacement field and $\bar{\mathbf{E}}$ and $\bar{\mathbf{D}}$ stand for the field values in the effective layer. The fundamental guided mode is phase and amplitude invariant along the x direction, so Eq. (15) is expressed as

$$d\int_{z=0}^{z=h} \bar{\epsilon}\bar{E}^2 = w\int_{z=0}^{z=h} \epsilon_{\mathrm{d}}E^2. \tag{16}$$

In addition, this equation is valid for all h and is further simplified to $\bar{E}^2 d\bar{\epsilon} = E^2 w\epsilon_{\mathrm{TM}}$. The property $E/\bar{E} = d/w$ is then used to obtain the effective permittivity

$$\bar{\epsilon} = \epsilon_{\mathrm{d}}\frac{d}{w}. \tag{17}$$

Eventually, the phase accumulated by a wave during its propagation through the structure is the same in both cases, $kh = \bar{k}h$. It is written as $\bar{\epsilon}\bar{\mu} = \epsilon_{\mathrm{TM}}$, where the effective layer is chosen to be magnetic. Its effective permeability can then be expressed due to Eq. (17):

$$\bar{\mu} = \frac{\epsilon_{\mathrm{TM}}}{\epsilon_{\mathrm{d}}}\frac{w}{d}. \tag{18}$$

In the reflection case [see Fig. 3(a)], the equivalent layer has to be deposited on a mirror, which displays an effective permittivity $\bar{\epsilon}_{\mathrm{m}}$. It is expressed by matching the reflection coefficients at the bottom of the slit:

$$\frac{\sqrt{\bar{\epsilon}/\bar{\mu}} - \sqrt{\bar{\epsilon}_{\mathrm{m}}}}{\sqrt{\bar{\epsilon}/\bar{\mu}} + \sqrt{\bar{\epsilon}_{\mathrm{m}}}} = \frac{\sqrt{\epsilon_{\mathrm{TM}}} - \sqrt{\epsilon_{\mathrm{m}}}}{\sqrt{\epsilon_{\mathrm{TM}}} + \sqrt{\epsilon_{\mathrm{m}}}}. \tag{19}$$

The effective permittivity of the metallic substrate is given by $\bar{\epsilon}_{\mathrm{m}} = \epsilon_{\mathrm{m}}/\bar{\mu}^2$.

We now consider the calculation of the effective nonlinear susceptibility $\bar{\chi}^{(2)}$, which can also be deduced from energy conservation. The original susceptibility $\chi^{(2)}$ is here considered as nondispersive as we are far from the material resonances, so the nonlinear part of the electric energy is simply given by $\mathbf{E}\cdot\mathbf{P}^{(2)}$. Its effective counterpart is therefore also considered as nondispersive, allowing us to obtain the expression

$$\bar{\chi}^{(2)} = \left(\frac{d}{w}\right)^2 \chi^{(2)}. \tag{20}$$

The nondispersive expression for the constitutive parameters of the effective medium are used in the following to analyze the linear and nonlinear behaviors of the structures.

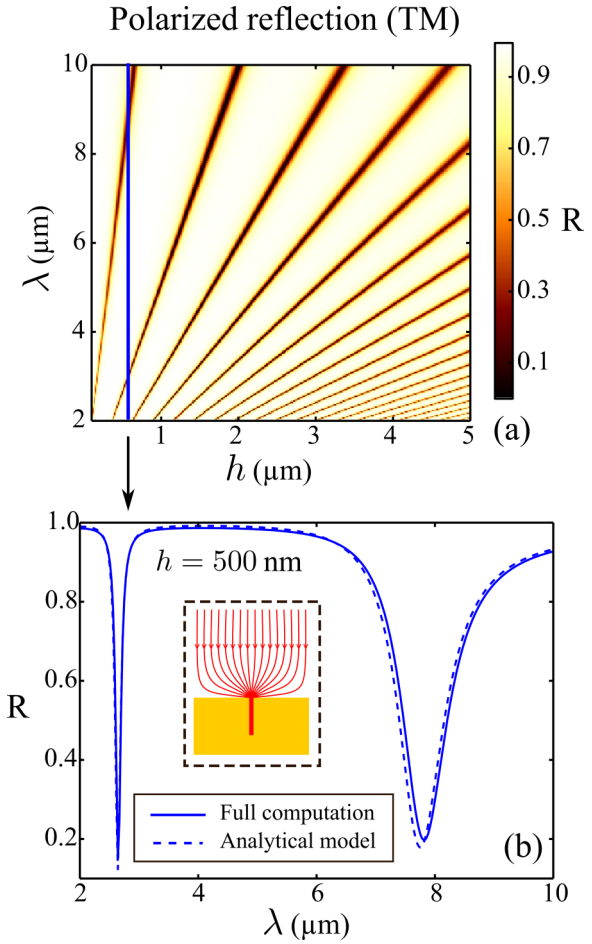

FIG. 4. (a) Reflectivity map as a function of the wavelength λ and the thickness h for the reflection. (b) Reflectivity as a function of the wavelength at a selected $h = 500$ nm. The dashed line represents the result obtained with the effective-medium model and the solid line shows the full computation with the original resonator. The parameters are $w = 200$ nm and $d = 1$ μm. The dielectric is gallium arsenide and the metal is gold.

C. Comparative results

In the following, the asymmetric resonator has a period $d = 1$ μm, a width $w = 0.2$ μm, and a height $h = 0.5$ μm. As previously stated, the metal is gold, described by a Drude model [19], and the dielectric is gallium arsenide, described by a Sellmeier model [18]. All the parameters are identical for the transmission case apart from the height $h = 1$ μm. The computations are performed with the B-spline modal method, which makes a fast and exact resolution of Maxwell equations and determines the nonlinear behavior under the undepleted pump approximation [27,28].

Reflection spectra for the reflection structure are shown for wavelengths ranging from 2 μm to 10 μm in Fig. 4(a) with varying thickness h. The Fabry-Pérot resonances are visible on this reflectivity map at the harmonic wavelengths. This behavior holds for growing values of thickness and no assumption about the value of h compared to the wavelength λ is needed to establish the effective-medium model. Shown below the reflectivity map is a comparison between this model (dashed lines) and the full numerical computation for the structured resonator [see Fig. 4(b)], where the results are found to be in very good agreement. The streamlines of the Poynting vector are shown in the insets at resonance for better clarity. All the energy is funneled into the groove, where it is absorbed for this reflection resonator. The transmission case also displays a very good comparison between the effective medium and the original structure for both its reflectivity and transmissivity (data not shown). The sole difference lies in the fact that the light is funneled through the slit for this transmission resonator and the streamlines below the structure only convey the transmitted energy (nearly 30% of the incoming energy, while the rest is either reflected or absorbed by the metallic sidewalls).

This analytical model renders very well metal-dielectric slits structures in TM illumination far from material resonances where losses are negligible and in the spectral range where the metal follows a Drude model. Moreover, in this spectral range, the studied resonators bring geometrical dispersion to the effective parameters, which makes frequency dispersion appear negligible. Indeed, superimposition of Fabry-Pérot resonances at the involved wavelengths of a given frequency conversion scheme respect the Rayleigh criterion, suggesting promising situations of mode matching. Following this idea, it has been shown that a first-order nondispersive approach correctly fits the solution that is obtained through the Landau formula for the electromagnetic energy.

IV. NONLINEAR ENHANCEMENT AND MODE MATCHING

We recall the expression for the effective nonlinear susceptibility $\bar{\chi}^{(2)}/\chi_d^{(2)} = (d/w)^2$, illustrating the great enhancement of the quantity of nonlinear sources inside the cavity of such structures. However, the nonlinear susceptibility is not the only parameter involved in the efficiency of frequency conversion processes. Due to the high value of the effective permittivity, for most of the wavelengths there is no impedance matching for the Fabry-Pérot cavity, which might result in a poor efficiency of the nonlinear processes. For a better understanding, the efficiency of the second-harmonic generation is computed for both structures in Fig. 5, using analytic expressions [29]. For the sake of comparison, the plotted efficiency is normalized by the intensity of a nonpatterned gallium arsenide layer, whose thickness is chosen so as to display Fabry-Pérot resonances at the same wavelengths. Following Eqs. (4) and (5), the equivalent gallium arsenide layer is a bit thicker than the patterned layer. The relative conversion efficiency is defined in reflection as

$$\eta^R = \frac{I^R_{\text{out}}}{I^R_{\text{out,ref}}}, \tag{21}$$

where I^R_{out} is the output reflected nonlinear intensity from the metal-dielectric structure computed with the analytical model and $I^R_{\text{out,ref}}$ is the reflected nonlinear intensity for a homogeneous layer of gallium arsenide exhibiting a fundamental Fabry-Pérot resonance at the same wavelength as the effective-medium layer [see Eq. (5)]. Due to Eq. (4), the gallium arsenide layer is slightly thicker than the effective-medium layer.

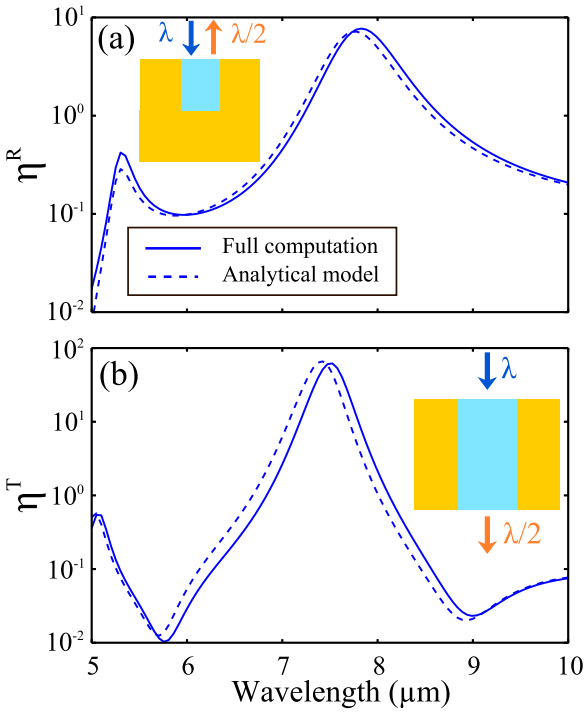

FIG. 5. The SHG relative conversion efficiencies of the structure in (a) reflection η^R and (b) transmission η^T, as functions of the pump wavelength. Solid lines represent the full computation and dashed lines show the analytical model. The parameters are $d = 1$ μm, $w = 0{,}2$ μm, and $h = 0.5$ μm for reflection case and $h = 1$ μm for transmission case.

In Fig. 5, two noticeable behaviors corresponding to resonant and nonresonant cases appear. First, at resonance, the maximum of the second-harmonic efficiency is indeed one order of magnitude greater, leading to interesting resonant values of the enhancement. The efficiency peaks are visible at the harmonic wavelengths. Second, the ratio can drop below 1, meaning that nonresonant behavior gives worse results for the structured resonators. This stems from the absence of impedance matching between the one of the cavity $Z = \sqrt{\bar{\mu}/\bar{\epsilon}}$ and the one of the outer medium. The second-harmonic light is hardly driven to the outer medium compared to the homogeneous layer case, leading to poor values of efficiency away from the resonance. Interestingly, the symmetric case leads to a better conversion efficiency in both reflection (data not shown) and transmission. This is a direct consequence of the presence of harmonics resonance at wavelengths given by Eq. (5), which may result in mode-matching situations where both the pump wavelength and the second-harmonic signal are at resonance. To fully understand these observations, the various scenarios of resonant behaviors in both structures for SHG (or DFG) are investigated in more detail below.

Figure 6 shows the three resonant situations that happen in the case of SHG with the respective conversion efficiency spectra. The relative conversion efficiency in transmission η^T is defined in a way similar to the reflection case. On the one hand, the incoming pump wave at wavelength λ_{pump} can be resonant to increase the quantity of created nonlinear polarization [Fig. 6(a)]. On the other hand, the outgoing signal wave at λ_{SHG} can be resonant to enhance the coupling from the slit to the outer medium [Fig. 6(b)]. When both conditions are fulfilled, it is a mode-matching situation [Fig. 6(c)] where the nonlinear intensity ratio reaches its highest value for a selected period. In the asymmetric resonator, only the cases of Figs. 6(a) and 6(b) can happen, thus limiting the value of η to the one obtained when the pump is solely resonant. Using a resonance at the second-harmonic wavelength is typically one order of magnitude less efficient, since the energy generated at the second harmonic depends only linearly on the

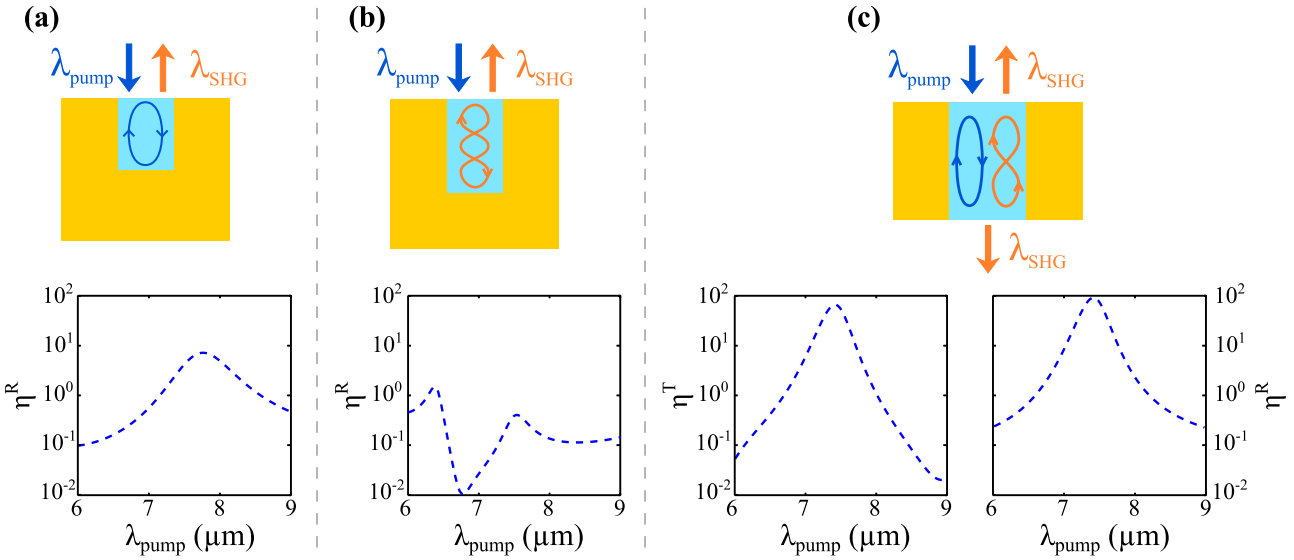

FIG. 6. Three scenarios of resonant behaviors for SHG in the metal-dielectric layer: (a) resonant pump ($h = 0.5$ μm and $h_{\text{GaAs}} = 0.55$ μm) or (b) resonant signal ($h = 0.73$ μm and $h_{\text{GaAs}} = 0.82$ μm) in a reflection resonator and (c) both resonant pump and signal ($h = 1$ μm and $h_{\text{GaAs}} = 1.15$ μm) in a transmission resonator creating a mode-matching configuration. Shown on the bottom are the corresponding SHG relative conversion efficiencies in (a) and (b) reflection η^R and (c) transmission η^T as functions of the pump wavelength. In the three cases, $d = 1$ μm and $w = 0{,}2$ μm.

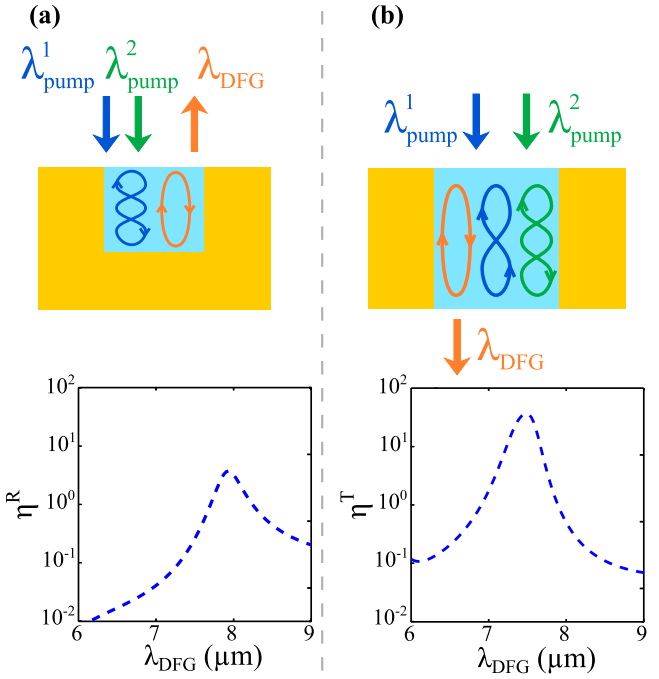

FIG. 7. Two scenarios of modes matching for DFG: (a) two modes matching with one resonant pump and a resonance at the DFG signal in a reflection resonator ($h = 0.5$ μm and $h_{GaAs} = 0.55$ μm) and (b) three modes matching (both resonant pumps and resonant DFG signal) in a transmission resonator ($h = 1$ μm and $h_{GaAs} = 1.15$ μm). Shown on the bottom are the corresponding DFG relative conversion efficiencies in (a) reflection η^R and (b) transmission η^T as functions of the DFG wavelength. The other parameters are the same in both structures ($d = 1$ μm and $w = 0.2$ μm).

second-harmonic electric field. In the case of the symmetric resonator, there is always a mode-matching situation for SHG between the fundamental resonance at λ and the first order of resonance at $\lambda/2$. The low-quality factors of both resonances can compensate for the natural dispersion of the material.

There are various configurations of mode matching in both structures for DFG. Two of them are illustrated in the case of the asymmetric (symmetric) resonator in Fig. 7(a) [Fig. 7(b)]. In both resonators, there is a degree of freedom to choose the wavelengths in order to be in a two-mode-matching situation. For instance, the signal wavelength λ_{DFG} determines the geometry of the resonator and one pump wavelength is chosen so as to match one of the harmonics of the resonator while the last one is determined by the energy-conservation condition. The conversion efficiency shown in Fig. 7(a) is comparable to the one obtained for SHG in Fig. 6(a), because the pump is degenerate so it could be considered as a degenerate two-mode-matching configuration. Three modes matching can be straightforwardly obtained in the symmetric resonator. Indeed, Eq. (5) quantifies the energy of each harmonic wavelength as a multiple of the fundamental wavelength energy. So, if two of the wavelengths involved in the DFG process have been chosen at resonance wavelengths, the third one is also at another resonance wavelength due to the energy-conservation condition (and neglecting the dispersivity). In Fig. 7(b), the fundamental wavelength and the two first-harmonic wavelengths are used ($\lambda^1_{pump} = \lambda_{DFG}/3$ and $\lambda^2_{pump} = \lambda_{DFG}/2$). As expected, it leads to a higher efficiency conversion ratio than in the two-mode-matching situation for both transmission and reflection (data not shown). However, this enhancement is lower than for the SHG, since the natural dispersion of the material must be managed for three different wavelengths.

In the optimal mode-matching situation for SHG, the metal-dielectric structure acts, at one particular pump wavelength, as a metasurface, which is described by the effective-medium model. Such a configuration is obtained here with the parameters $\lambda_{pump} = 7.8$ μm, $w = 200$ nm, $h = 500$ nm, and $d = 1$ μm as shown in Fig. 5(a). To compare our structure with a previously reported metasurface from the literature, we compute the absolute value of our SHG conversion efficiency for an impinging pump plane wave carrying an intensity of 10 kW cm^2, with the nonlinear susceptibility of gallium arsenide $\chi^{(2)} = (2/\sqrt{3})150$ pm/V according to Ref. [30]. The absolute SHG conversion efficiency is then found to be equal to 5×10^{-4} with an effective nonlinear susceptibility of $\bar{\chi}^{(2)} = 4.3$ nm/V, which is of the same order as the reported value 2×10^{-4} under a Gaussian focused beam [7]. Such a metal-dielectric component is thus able to greatly enhance nonlinear generation through lateral field confinement within a volume of semiconductor displaying a second-order susceptibility.

V. CONCLUSION

To conclude, nonlinear phenomena in subwavelength metallic slits or grooves filled with a nonlinear material can be fairly described by this homogenization model. This metasurface exhibits an unusually high nonlinear effective susceptibility that leads to higher efficiency of the frequency conversion processes and is further enhanced by exploiting mode matching between resonances. The effective-medium properties can be spatially tuned, by simply changing the in-plane geometrical parameters, making it possible, for instance, to address various wavelength ranges. These results can be directly applied to various metals and nonlinear dielectric materials. In the midinfrared range, the efficiency for a thick layer of the effective medium is plagued by the Ohmic metallic losses, but it is no longer the case for higher-wavelength ranges.

ACKNOWLEDGMENTS

We acknowledge financial support from the ONERA through the Moliere project and from a DGA-MRIS scholarship.

[1] A. A. Zharov, I. V. Shadrivov, and Y. S. Kivshar, Phys. Rev. Lett. **91**, 037401 (2003).

[2] W. Cai, U. K. Chettiar, A. V. Kildishev, and V. M. Shalaev, Nat. Photon. **1**, 224 (2007).

[3] A. Rose, D. Huang, and D. R. Smith, Phys. Rev. Lett. **107**, 063902 (2011).
[4] M. Kauranen and A. V. Zayats, Nat. Photon. **6**, 737 (2012).
[5] R. Czaplicki, H. Husu, R. Siikanen, J. Mäkitalo, M. Kauranen, J. Laukkanen, J. Lehtolahti, and M. Kuittinen, Phys. Rev. Lett. **110**, 093902 (2013).
[6] M. Lapine, I. V. Shadrivov, and Y. S. Kivshar, Rev. Mod. Phys. **86**, 1093 (2014).
[7] J. Lee, M. Tymchenko, C. Argyropoulos, P.-Y. Chen, F. Lu, F. Demmerle, G. Boehm, M.-C. Amann, A. Alù, and M. A. Belkin, Nature (London) **511**, 65 (2014).
[8] A. E. Minovich, A. E. Miroshnichenko, A. Y. Bykov, T. V. Murzina, D. N. Neshev, and Y. S. Kivshar, Laser Photon. Rev. **9**, 195 (2015).
[9] F. X. Wang, F. J. Rodríguez, W. M. Albers, R. Ahorinta, J. E. Sipe, and M. Kauranen, Phys. Rev. B **80**, 233402 (2009).
[10] P. Genevet, J.-P. Tetienne, E. Gatzogiannis, R. Blanchard, M. A. Kats, M. O. Scully, and F. Capasso, Nano Lett. **10**, 4880 (2010).
[11] K. Thyagarajan, J. Butet, and O. J. Martin, Nano Lett. **13**, 1847 (2013).
[12] J. E. Sipe and R. W. Boyd, Phys. Rev. A **46**, 1614 (1992).
[13] D. R. Smith and J. B. Pendry, J. Opt. Soc. Am. B **23**, 391 (2006).
[14] S. Larouche and D. R. Smith, Opt. Commun. **283**, 1621 (2010).
[15] S. Park, J. W. Hahn, and J. Y. Lee, Opt. Express **20**, 4856 (2012).
[16] M. Celebrano, X. Wu, M. Baselli, S. Großmann, P. Biagioni, A. Locatelli, C. De Angelis, G. Cerullo, R. Osellame, B. Hecht, L. Duò, F. Ciccacci, and M. Finazzi, Nat. Nanotechnol. **10**, 412 (2015).
[17] O. Wolf, S. Campione, A. Benz, A. P. Ravikumar, S. Liu, T. S. Luk, E. A. Kadlec, E. A. Shaner, J. F. Klem, M. B. Sinclair, and I. Brener, Nat. Commun. **6**, 7667 (2015).
[18] T. Skauli, P. Kuo, K. Vodopyanov, T. Pinguet, O. Levi, L. Eyres, J. Harris, M. Fejer, B. Gerard, L. Becouarn, and E. Lallier, J. Appl. Phys. **94**, 6447 (2003).
[19] R. L. Olmon, B. Slovick, T. W. Johnson, D. Shelton, S.-H. Oh, G. D. Boreman, and M. B. Raschke, Phys. Rev. B **86**, 235147 (2012).
[20] S. Collin, F. Pardo, and J. Pelouard, Opt. Express **15**, 4310 (2007).
[21] F. Pardo, P. Bouchon, R. Haïdar, and J.-L. Pelouard, Phys. Rev. Lett. **107**, 093902 (2011).
[22] P. Bouchon, F. Pardo, B. Portier, L. Ferlazzo, P. Ghenuche, G. Dagher, C. Dupuis, N. Bardou, R. Haïdar, and J. Pelouard, Appl. Phys. Lett. **98**, 191109 (2011).
[23] P. Lalanne and J.-P. Hugonin, J. Opt. Soc. Am. A **15**, 1843 (1998).
[24] J.-T. Shen, P. B. Catrysse, and S. Fan, Phys. Rev. Lett. **94**, 197401 (2005).
[25] D. J. Ironside and J.-T. Shen, Appl. Phys. Lett. **102**, 021907 (2013).
[26] L. D. Landau, J. Bell, M. Kearsley, L. Pitaevskii, E. Lifshitz, and J. Sykes, *Electrodynamics of Continuous Media* (Elsevier, Amsterdam, 1984), Vol. 8.
[27] P. Bouchon, F. Pardo, R. Haïdar, and J. Pelouard, J. Opt. Soc. Am. A **27**, 696 (2010).
[28] S. Héron, F. Pardo, P. Bouchon, J.-L. Pelouard, and R. Haïdar, J. Opt. Soc. Am. B **32**, 275 (2015).
[29] J. Van Der Ziel, IEEE J. Quantum Electron. **12**, 407 (1976).
[30] T. Skauli, K. Vodopyanov, T. Pinguet, A. Schober, O. Levi, L. Eyres, M. Fejer, J. Harris, B. Gerard, L. Becouarn, E. Lallier, and G. Arisholm, Opt. Lett. **27**, 628 (2002).